ACS Chemical Neuroscience

pubs.acs.org/chemneuro

Research Article

Synthesis, Biodistribution, and Radiation Dosimetry of a Novel mGluR5 Radioligand: ^{18}F-AZD9272

Sangram Nag,* Katarina Varnäs, Ryosuke Arakawa, Mahabuba Jahan, Magnus Schou, Lars Farde, and Christer Halldin

Cite This: *ACS Chem. Neurosci.* 2020, 11, 1048−1057

Read Online

ACCESS | Metrics & More | Article Recommendations

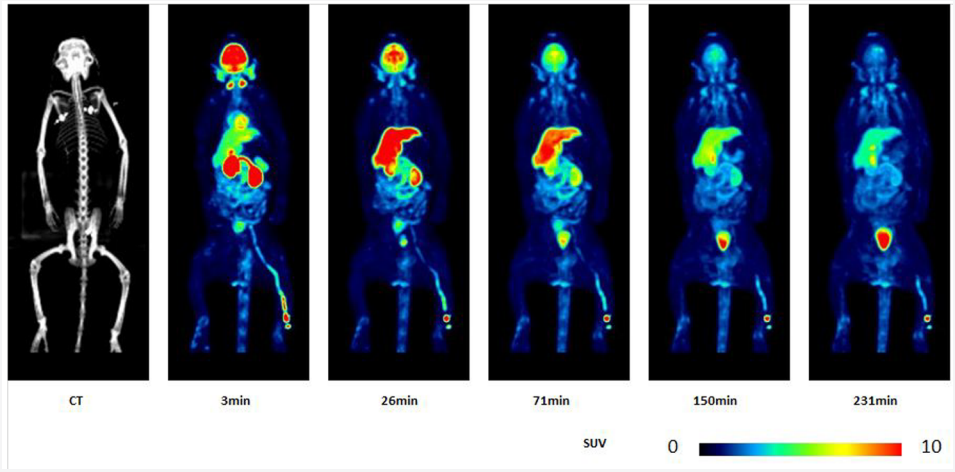

ABSTRACT: The metabotropic glutamate receptor subtype mGluR5 has been proposed as a potential drug target for CNS disorders such as anxiety, depression, Parkinson's disease, and epilepsy. The AstraZeneca compound AZD9272 has previously been labeled with carbon-11 and used as a PET radioligand for mGluR5 receptor binding. The molecular structure of AZD9272 allows one to label the molecule with fluorine-18 without altering the structure. The aim of this study was to develop a fluorine-18 analogue of AZD9272 and to examine its binding distribution in the nonhuman primate brain *in vivo* as well as to obtain whole body radiation dosimetry. ^{18}F-AZD9272 was successfully synthesized from a nitro precursor. The radioligand was stable, with a radiochemical purity of >99% at 2 h after formulation in a sterile phosphate buffered solution (pH = 7.4). After injection of ^{18}F-AZD9272 in two cynomolgus monkeys, the maximum whole brain radioactivity concentration was 4.9−6.7% of the injected dose (n = 2) and PET images showed a pattern of regional radioactivity consistent with that previously obtained for ^{11}C-AZD9272. The percentage of parent radioligand in plasma was 59 and 64% (n = 2) at 120 min after injection of ^{18}F-AZD9272, consistent with high metabolic stability. Two whole body PET scans were performed in nonhuman primates for a total of 231 min after injection of ^{18}F-AZD9272. Highest uptakes were seen in liver and small intestine, followed by brain and kidney. The estimated effective dose was around 0.017 mSv/MBq. ^{18}F-AZD9272 shows suitable properties as a PET radioligand for *in vivo* imaging of binding in the primate brain. ^{18}F-labeled AZD9272 offers advantages over ^{11}C-AZD9272 in terms of higher image resolution, combined with a longer half-life. Moreover, based on the distribution and the estimated radiation burden, imaging of ^{18}F-AZD9272 could be used as an improved tool for quantitative assessment and characterization of AZD9272 binding sites in the human brain by using PET.

KEYWORDS: *PET, mGluR5 radioligands, NHP, fluorine-18, kinetics, dosimetry*

INTRODUCTION

Glutamate is the brain's main excitatory neurotransmitter primarily located on the membranes of neuronal and glial cells and is present in over 50% of nervous tissue.[1] It is particularly abundant in the human nervous system and mostly prominent in the human brain. Glutamate acts through ionotropic (NMDA, kainite, and AMPA) and metabotropic glutamate

Received: December 20, 2019
Accepted: March 13, 2020
Published: March 13, 2020

https://dx.doi.org/10.1021/acschemneuro.9b00680
ACS Chem. Neurosci. 2020, 11, 1048−1057

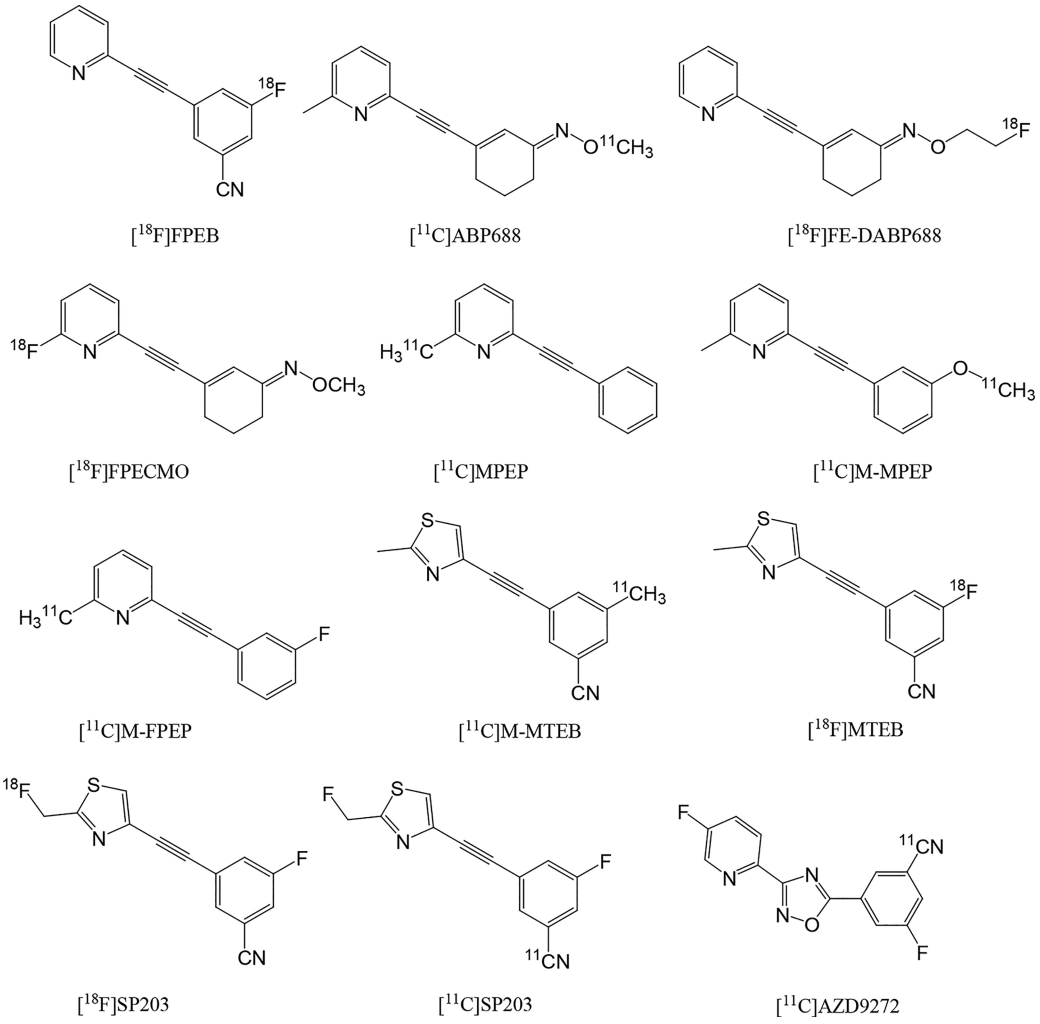

Figure 1. Structures of mGluR5 PET radioligands.

(mGlu) receptor subtypes and affects cells through a signal transduction cascade.[2]

Metabotropic glutamate receptors (mGluRs) are a family of G protein-coupled receptors. In 1992, mGluR5 was first cloned in animals and followed by humans several years later.[3] Even though its actions are mostly excitatory,[4] there are strong links and receptor interactions between mGluR5 and the NMDA receptor.[5] It has also been reported that the activation of mGluR5 enhances GABA, especially in the nucleus accumbens.[6] The density of mGluR5 is high primarily in the forebrain regions, striatum, and limbic regions.[7,8] Moreover, the density of mGluR5 is much higher in younger animals than in adults suggests that early intervention targeting the mGluR5 may lead to prevent the neurodevelopmental disorders.[9]

It is believed that presynaptic mGluR5 receptors participates in the regulation of synaptic plasticity and changes in neuronal excitability to maintain homeostasis.[10] Because of its functions in different neuronal processes, mGluR5 has been suggested as a therapeutic drug target for several neurological disorders such as Parkinson's diseases,[11,12] anxiety,[13,14] depression,[15] schizophrenia,[16] seizure disorder,[17] addiction[18] as well as various chronic pain states.[19]

Positron emission tomography (PET) has been widely utilized in visualizing the localization of mGluR5. Imaging brain mGluR5 with PET in humans has been useful for studying neurodegenerative disorders and addiction.[20] Several radioligands (Figure 1) [^{18}F]FPEB,[21] ^{11}C-ABP688,[22] ^{18}F-FPECMO,[23] ^{11}C-MPEP,[24] ^{11}C-M-FPEP,[25] ^{11}C-M-MTEB,[25] ^{18}F-SP203,[26] ^{18}F-MTEB,[27] ^{11}C-SP203,[28] and ^{18}F-FE-DABP688[29] have been developed and applied preclinically or clinically to image brain mGluR5. Most of those are diaryl alkynes, structural analogues of the prototype mGluR5 NAM MPEP. A noncompetitive mGluR5 antagonist AZD9272 which does not depend on the presence of alkyne moiety was developed by AstraZeneca.[30] AZD9272 was previously labeled with carbon-11 and evaluated as a potential mGluR5 radioligand in nonhuman primates (NHPs) and human subjects.[31,32] However, due to the short half-life of carbon-11 (20.4 min), the use of such a radioligand is restricted to imaging facilities that are close to the site of production. In addition, a three step synthesis of ^{11}C-AZD9272 using palladium mediated ^{11}C-cyanation was associated with difficulties in automation.[31]

Since AZD9272 has two fluorine functional groups, it allows the radiolabeling with ^{18}F from the corresponding nitro-precursor without altering the structure. Fluorine-18 labeled PET tracers may provide advantages for use in PET imaging. Relatively long half-life (109.8 min) facilitates imaging at later time-points and lower positron energy (0.635 MeV) allows higher intrinsic resolution in the PET images. Fluorine-18

https://dx.doi.org/10.1021/acschemneuro.9b00680
ACS Chem. Neurosci. 2020, 11, 1048−1057

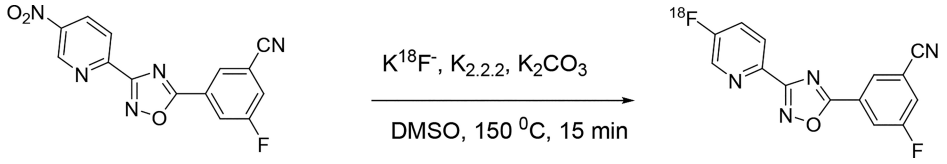

Figure 2. Radiosynthesis of ^{18}F-AZD9272.

labeled radiotracers can be prepared in multiple clinical doses for long-distance distribution, enabling widespread clinical use.

The objectives of the present PET-study were to (i) to develop a fast and efficient synthetic method for labeling of a mGluR5 ligand AZD9272 with fluorine-18, (ii) to evaluate its binding *in vivo* in the NHP brain, and (iii) to provide dosimetry estimates for ^{18}F-AZD9272 based on NHP whole-body PET measurements.

RESULTS AND DISCUSSION

Radiochemistry. The radiolabeling of ^{18}F-AZD9272 (3-fluoro-5-(3-(5-[^{18}F]fluoropyridin-2-yl)-1,2,4-oxadiazol-5-yl)-benzonitrile) was achieved by nucleophilic substitution of the corresponding nitro-precursor (3-fluoro-5-(3-(5-nitropyridin-2-yl)-1,2,4-oxadiazol-5-yl)benzonitrile) by ^{18}F-fluoride in the presence of $K_{2.2.2}$ and K_2CO_3 as shown in Figure 2. Different solvents such as acetonitrile, DMF, and DMSO were tested at different temperatures (Table 1). A combination of DMSO as the reaction solvent and 150 °C reaction temperature for 10 min resulted in the desired product with the best radiochemical yield. After HPLC purification, 1.9−3.2 GBq of ^{18}F-AZD9272 was obtained from 15−20 min irradiation at 35 μA. The average radiochemical yield of the radiosynthesis was 23% (nondecay corrected), and the radiochemical purity was higher than 99%. The overall radiosynthesis including the fluorination reaction, HPLC purification, SPE isolation, and radiotracer formulation was completed within 70−75 min. The identity of the labeled compound was confirmed by co-injection of their corresponding fluorine-19 analogue using analytical HPLC. The radioligand ^{18}F-AZD9272 was found to be stable in PBS buffered solution (pH = 7.4) for the duration of 120 min. ^{18}F-AZD9272 was obtained with a molar activity (MA) of 94 ± 103 GBq/μmol (n = 6) at the time of injection.

Table 1. Optimization of Radiolabeling of ^{18}F-AZD9272

entry	precursor (mg)	solvent	reaction time (min)	reaction temperature (°C)	yield (%)
1	2	acetonitrile	5	75	1
				90	1
				110	3
			15	75	1
				90	1
				110	5
			30	90	2
				100	5
2	2	DMSO	5	90	0
				120	1
				135	3
				150	5
			10	90	0
				120	1
				135	5
				150	5
			15	120	2
				135	6
				150	23
				165	22
			30	150	23
				165	23
3	4−6	DMSO	15	150	23
4	2	DMF	15	125	2
				145	15
			30	125	4
				145	17
				155	15

Brain PET. The injected radioactivity of ^{18}F-AZD9272 was 155 and 155 MBq for NHP1 and NHP2, respectively. The MA at the time of injection was 45 and 31 GBq/μmol, and the injected mass was 0.98 and 1.46 μg. Fusion images of MRI and summated PET of NHP2 are shown in Figure 3A. The uptake was highest in the striatum, lower in the thalamus and frontal cortex, and lowest in the cerebellum and occipital cortex. The corresponding regional brain time−activity curves (TACs) of NHP2 are shown in Figure 3B. The total distribution volume (V_T) obtained by the two tissue compartment (2TC) model and Logan graphical analysis (GA) using metabolite corrected plasma radioactivity are shown in Table 2. V_T's by GA are well correlated to those by 2TC although with slightly lower values (11% and 6%) (Figure 4A). Bias is quite small as within 3% at 75 min for both 2TC and GA (Figure 4B).

The brain uptake of ^{18}F-AZD9272 is consistent with that previously reported for ^{11}C-AZD9272.[33] Also, the V_T values obtained by 2TC are similar between ^{18}F-AZD9272 and ^{11}C-AZD9272, *e.g.*, 17.3 vs 18.0 mL/cm^3 (ventral striatum) and 5.7 vs 6.5 mL/cm^3 (occipital cortex).

V_T values estimated by GA were well correlated with those by 2TC, although slightly lower values were obtained. Additionally, a short length of measurement showed a small bias in V_T values obtained with both 2TC and GA. This indicates that GA with a short duration of measurement (*e.g.*, 75 min) could be used for the estimation for V_T of ^{18}F-AZD9272.

The consistent binding pattern observed with ^{18}F- and ^{11}C-labeled AZD9272 further confirms that the regional brain distribution for radiolabeled AZD9272 differs from that for other mGluR5 radioligands.[33] Observations reported elsewhere[31] suggest that AZD9272 displays additional, non-mGluR5-related binding that may represent specific binding to monoamine oxidase-B (MAO-B). Based on our previous observations,[31] close to 90% of specific binding for ^{18}F-AZD9272in NHP brain can be inhibited by administration of a MAO-B-selective ligand. Moreover, the MAO-B component of ^{11}C-AZD9272 binding has been estimated to be approximately 90−95% in human brain stem, thalamus, amygdala, cerebellum, and ventral striatum. The significant contribution MAO-B binding to the signal for AZD9272 suggests that ^{18}F-AZD9272could serve as a radioligand for assessment of MAO-B availability in these regions of the primate brain.

https://dx.doi.org/10.1021/acschemneuro.9b00680
ACS Chem. Neurosci. 2020, 11, 1048−1057

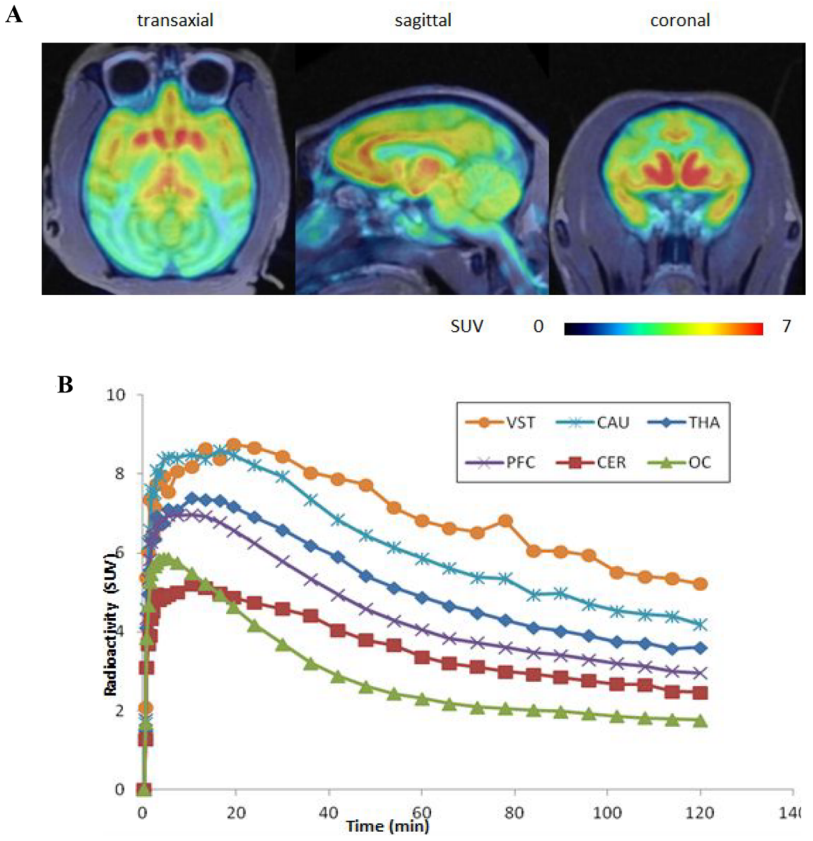

Figure 3. (A) PET images of ^{18}F-AZD9272 coregistered with MRI and averaged between 9 and 120 min in the transaxial (left), sagittal (middle), and coronal (right) projections. (B) Time−activity curves for ^{18}F-AZD9272in different brain regions.

Table 2. V_T Using the 2TC Model and GA with Metabolite Corrected Plasma Activity[a]

	2TC (mL/cm^3)			GA (mL/cm^3)		
	NHP1	NHP2	mean	NHP1	NHP2	mean
ACC	11.5	11.2	11.4	10.2	10.7	10.4
AMG	15.0	14.4	14.7	12.8	13.1	13.0
CAU	13.3	13.7	13.5	12.1	13.0	12.6
CER	7.1	7.9	7.5	6.6	7.6	7.1
HIP	10.7	11.9	11.3	9.7	11.2	10.5
INS	9.0	10.0	9.5	8.5	9.6	9.1
OC	5.4	6.0	5.7	5.5	5.7	5.6
PFC	9.6	9.5	9.5	8.9	9.3	9.1
PUT	9.5	10.7	10.1	9.3	10.1	9.7
TC	7.6	8.4	8.0	7.2	8.1	7.7
THA	11.7	11.4	11.6	10.6	10.8	10.7
VM	11.0	8.9	9.9	9.1	8.4	8.8
VST	17.3	17.3	17.3	14.5	15.6	15.1

[a]ACC, anterior cingulate cortex,; AMG, amygdala; CAU, caudate; CER, cerebellum; HIP, hippocampus; INS, insular cortex; OC, occipital cortex; PFC, prefrontal cortex; PUT, putamen; TC, temporal cortex; THA, thalamus; VM, ventral midbrain; VST, ventral striatum.

Nevertheless, characterization as a tracer for imaging brain MAO-B would require comparison of regional AZD9272 binding with that of established MAO-B radioligands in the same subjects. Taken together, ^{18}F-AZD9272 shows favorable properties in terms of improved stability and image resolution and offers advantages over ^{11}C-AZD9272 for further identification and characterization of AZD9272 binding to MAO-B.

Radiometabolite Analysis. The recovery of radioactivity from plasma into acetonitrile after deproteinization was higher than 95%. The parent compound was more abundant at 5 min representing approximately 95% and it decreased to 65% at 120 min (Figure 5A). The identity of the radio metabolite ^{18}F-AZD9272 was confirmed by coinjection with the authentic nonradioactive AZD9272. The similar time-course for radio metabolism was observed for ^{11}C-AZD9272 (Figure 5B).[33] HPLC analysis of plasma following injection of ^{18}F-AZD9272, parent compound and one radioactive metabolite was detected which eluted at 6.7 and 6.3 min (Figure 5C). The abundance of the radiometabolite at 6.3 min increases with time and representing approximately 4% at 5 min and it increased to 17% at 120 min. The identity of the radiometabolite was not analyzed. In principle, it is a possibility that the metabolite is sufficiently lipophilic to enter the brain. However, according to the time stability analysis, the bias to the duration of measurements was small (Figure 4B. This observation provides indirect support for the view that the radiometabolite is less likely to impact the quantitative estimates.

Whole Body PET. The injected radioactivity of ^{18}F-AZD9272 was 217 and 199 MBq for the two NHPs (NHP3 and NHP4) respectively. The MA at the time of injection was 41 and 58 GBq/μmol, and the injected mass was 1.53 and 0.97 μg. CT and PET images of maximum intensity projection (MIP) over time of NHP4 are shown in Figure 6 and the time activity curves of NHP4 are shown in Figure 7. High uptakes were seen in liver and small intestine, followed by brain and kidney. Human radiation dose estimates indicate that most organs appear to receive around 0.01−0.02 mSv/MBq (Table

https://dx.doi.org/10.1021/acschemneuro.9b00680
ACS Chem. Neurosci. 2020, 11, 1048−1057

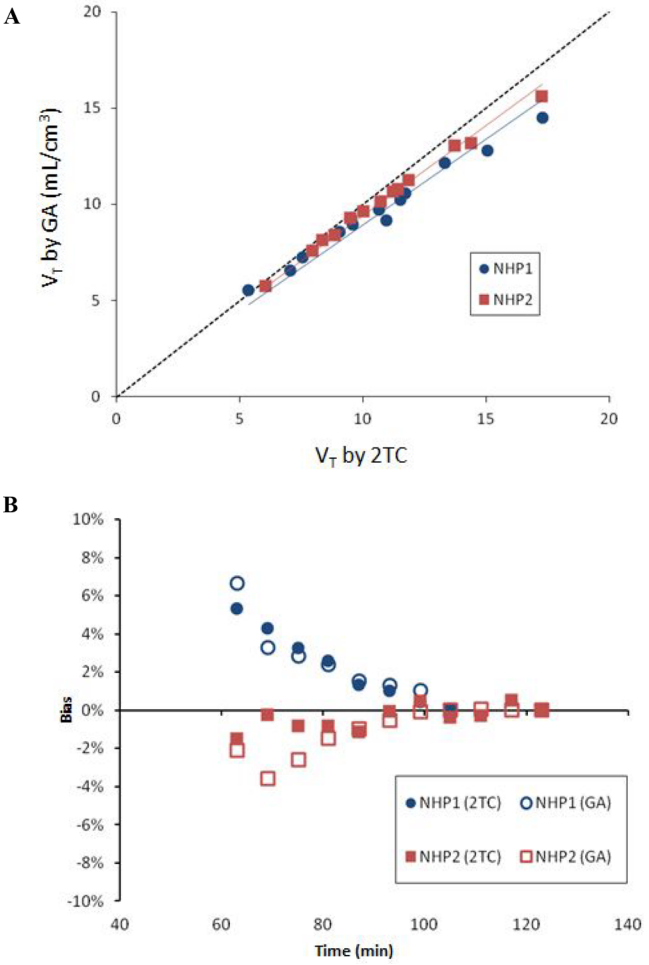

Figure 4. (A) Correlation of V_T values obtained with 2TC model and GA with metabolite corrected plasma radioactivity. (B) Time stability of V_T to the maximum duration of 105 min (NHP1) and 123 min (NHP2).

3). The upper large intestine (ULI) wall appears to receive the highest dose, around 0.068 mSv/MBq.

The estimated radiation dose of ^{18}F-AZD9272 was 0.017 mSv/MBq which is similar to that of other ^{18}F-labeled radioligands such as ^{18}F-FDG (0.015−0.029 mSv/MBq) and ^{18}F-AV-45 (0.016−0.020 mSv/MBq).[34] It means that 570 MBq can be injected to humans if the limit is 10 mSv for the total radiation exposure. It would allow multiple PET examinations on the same research subject in studies of the human brain.

CONCLUSION

The present study demonstrated that the radioligand ^{18}F-AZD9272 can be efficiently labeled with fluorine-18. A PET measurement in two cynomolgus monkey showed high brain uptake which is similar to the previously developed radioligand ^{11}C-AZD9272. The estimated radiation burden of ^{18}F-AZD9272 was 0.017 mSv/MBq based on the distribution which may allow repeated scans in the same human subject. ^{18}F-AZD9272 offers advantages over ^{11}C-AZD9272 for further identification and characterization of potential AZD9272 binding to MAO-B.

MATERIALS AND METHODS

General. Liquid chromatographic analysis (LC) was performed with a Merck-Hitachi gradient pump and a Merck-Hitachi, L-4000 variable wavelength UV-detector. LC-MS was performed using a Waters Quattra-Tof Premier micro mass spectrometer, or Waters SQD 3001 single quadrupole mass spectrometer, coupled to Waters Acquity UPLC instruments. The precursor (3-fluoro-5-(3-(5-nitropyridin-2-yl)-1,2,4-oxadiazol-5-yl)benzonitrile) and the reference standard nonradioactive AZD9272 (3-fluoro-5-(3-(5-fluoropyridin-2-yl)-1,2,4-oxadiazol-5-yl)benzonitrile) were supplied by AstraZeneca AB. All other chemicals and reagents were obtained from commercial sources and used without any further purification. Solid-phase extraction (SPE) cartridges SepPak QMA light and SepPak C18 Plus were purchased from Waters (Milford, MA). The C18 Plus cartridge was activated using EtOH (10 mL) followed by sterile water (10 mL). The SPE cartridge SepPak QMA light was activated using K_2CO_3 solution (0.5M, 10 mL) followed by water (15 mL, 18 MΩ,). Fluorine-18 fluoride was produced at Karolinska Hospital (Stockholm, Sweden)

Production of ^{18}F-Fluoride (^{18}F−F$^-$). Fluorine-18 fluoride (^{18}F−F$^-$) was produced from a GEMS PET trace Cyclotron using 16.4 MeV protons via the ^{18}O(p,n)^{18}F nuclear reaction on ^{18}O-enriched water (^{18}O−H_2O). After irradiation, ^{18}F−F$^-$ was isolated from ^{18}O−H_2O on a light anion exchange cartridge (SepPak QMA) and subsequently eluted from the cartridge with a solution of K_2CO_3 (9.75 μmol, 1.35 mg), Kryptofix$_{2.2.2}$ (4,7,13,16,21,24-hexaoxa-1,10-diazabicyclo-[8.8.8]hexacosane-K$_{2.2.2}$) (19.5 μmol, 7.35 mg) in water (64 μL, 18 MΩ), and MeCN (1.5 mL) to a 10 mL screw cap reaction vessel. The solvents were evaporated at 150 °C for 10 min under continuous nitrogen flow (70−80 mL/min) to form a dry complex of ^{18}F−F$^-$/K_2CO_3/K$_{2.2.2}$. The residue was cooled to room temperature (RT) before the precursor (3-fluoro-5-(3-(5-nitropyridin-2-yl)-1,2,4-oxadiazol-5-yl)benzonitrile) was added.

Synthesis of ^{18}F-AZD9272 (3-Fluoro-5-(3-(5-[^{18}F]-fluoropyridin-2-yl)-1,2,4-oxadiazol-5-yl)benzonitrile). To the dry complex of ^{18}F−F-/K_2CO_3/K$_{2.2.2}$, nitro-precursor (3-fluoro-5-(3-(5-nitropyridin-2-yl)-1,2,4-oxadiazol-5-yl)benzonitrile) (2 mg) in DMSO (500 μL) was added at 150 °C and left for 15 min to produce ^{18}F-AZD9272. The reaction mixture was cooled to RT and was diluted with water to a total volume of 3 mL before injecting to a semipreparative reverse phase μ-Bondapak HPLC column (C18, 7.8 Ø × 300 mm, 10 μm, Waters) for purification. The column outlet was connected to an UV absorbance detector (λ = 270 nm) in series with a GM tube for radioactivity detection. Elution with mobile phase CH_3CN/10 mM H_3PO_4 (40/60) at a flow rate of 5 mL/min gave a radioactive fraction corresponding to pure ^{18}F-AZD9272 (retention time 28−30 min). The fraction was diluted with water (50 mL, 18 MΩ), and the resulting mixture was loaded on to a preconditioned (10 mL of ethanol followed by 10 mL of sterile water) SepPak tC18 plus cartridge. The cartridge was washed with sterile water (10 mL), and the isolated product, ^{18}F-AZD9272, was eluted with 1 mL of ethanol into a sterile vial containing phosphate buffered saline solution (PBS, 9 mL).

Quality Control of ^{18}F-AZD9272. The radiochemical purity, identity, and stability of ^{18}F-AZD9272 was determined by using an analytical HPLC system which included a ACE RP column (C18, 3.9 Ø × 250 mm, 5 μm particle size), Merck-Hitatchi L-7100 Pump, L-7400 UV detector, and GM tube for radioactivity detection (VWR International). The mobile phase CH_3CN/0.1% TFA with a gradient HPLC method (10−90% in 8 min) and flow rate of 3 mL/min was used to elute the product. The effluent was monitored with a UV absorbance detector (λ = 270 nm) coupled to a radioactive detector (b-flow, Beckman, Fullerton, CA). The retention time (Rt) of ^{18}F-AZD9272 was 4−5 min. The identity of ^{18}F-AZD9272 was confirmed by using HPLC with the coinjection of the authentic nonradioactive AZD9272 (3-fluoro-5-(3-(5-fluoropyridin-2-yl)-1,2,4-oxadiazol-5-yl)-benzonitrile) standard.

Molar Activity (MA) Determination. The MA of the final product was measured by analytical HPLC which included a ACE RP

https://dx.doi.org/10.1021/acschemneuro.9b00680
ACS Chem. Neurosci. 2020, 11, 1048−1057

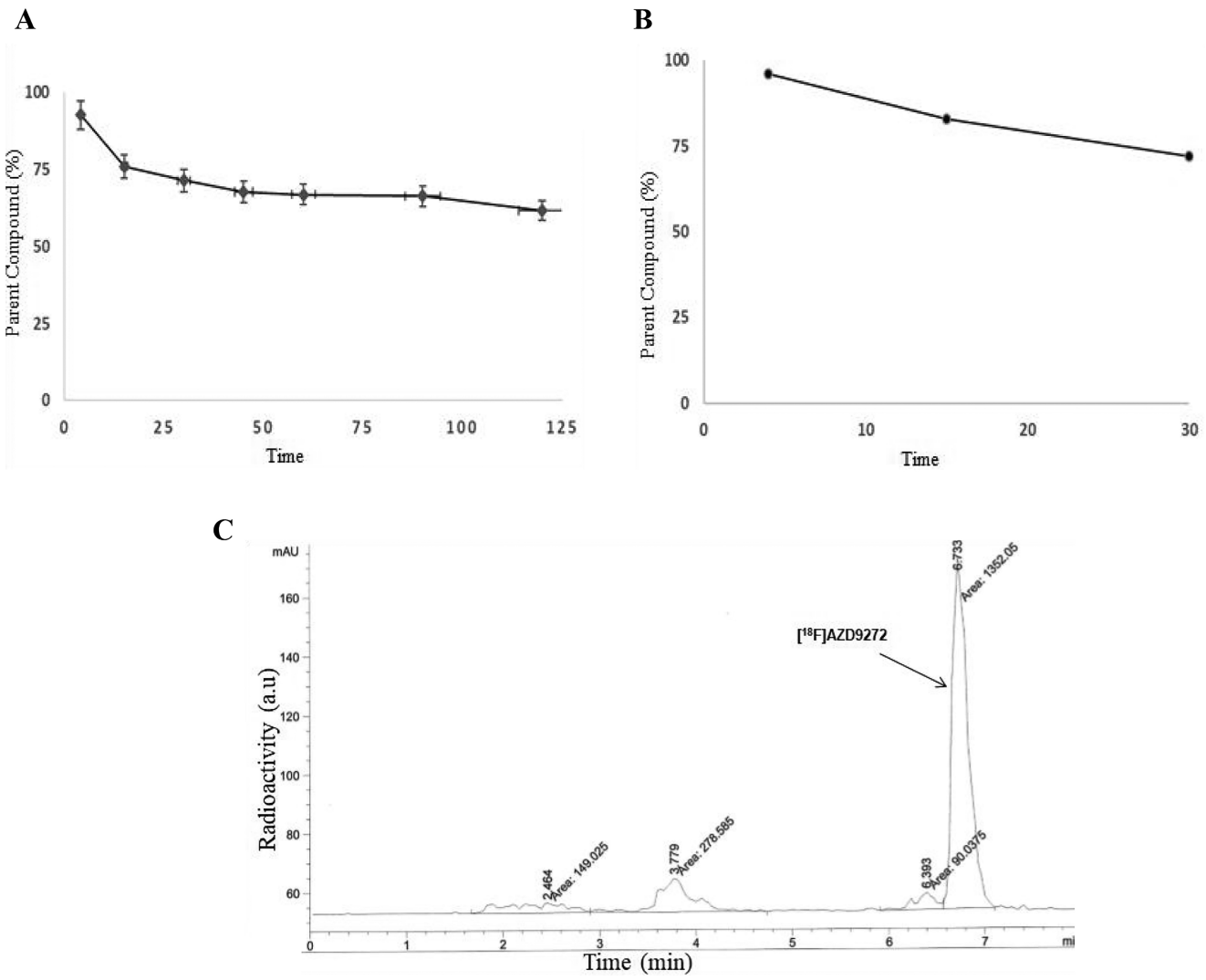

Figure 5. Radiometabolite analysis during the course of the PET measurements. It is shown as the relative plasma composition of radiometabolites and parent compound in percent of total plasma radioactivity that was injected. (A) *In vivo* radiometabolism of ^{18}F-AZD9272 was detected during the 120 min PET scan. (B) *In vivo* radiometabolism of ^{11}C-AZD9272 was detected during the 30 min PET scan. (C) Representative HPLC chromatogram 15 min after injection of ^{18}F-AZD9272.

column (C18, 3.9 Ø × 250 mm, 5 μm particle size) using mobile phase CH_3CN/50 mM H_3PO_4 (35/65) and flow rate of 2 mL/min. MA was calibrated for UV absorbance (λ = 270 nm) response per mass of ligand and calculated as the radioactivity of the radioligand (GBq) divided by the amount of the associated carrier substance (μmol). Each sample was analyzed three times and compared to a reference standard also analyzed three times.

PET Measurements in a Cynomolgus Monkey. The study was approved by the Animal Ethics Committee of the Swedish Animal Welfare Agency (Dnr N185/14) and was performed according to "Guidelines for planning, conducting and documenting experimental research" (Dnr 4820/06-600) of Karolinska Institutet. The NHPs were housed in the Astrid Fagraeus Laboratory (AFL) of the Swedish Institute for Infectious Disease Control, Solna, Sweden.

Brain PET. Two male cynomolgus monkeys (NHP1: 5460 g and NHP2: 7080 g) were used in this study. Parts of the data have been reported.[32] Anesthesia was induced by intramuscular injection of ketamine hydrochloride (approximately 10 mg/kg) at AFL and maintained by intravenous infusion of ketamine (4 mg/kg/h) and xylazine (0.4 mg/kg/h) with a pump. The NHP head was immobilized with a fixation device. Body temperature was maintained by using a Bair Hugger system (model 505, Arizant Healthcare, MN) and monitored with an esophageal thermometer. Heart rate, blood pressure, respiratory rate, and oxygen saturation were continuously monitored throughout the experiments. Fluid balance was maintained by continuous infusion of saline.

PET measurements were conducted using a High Resolution Research Tomograph (HRRT) PET scanner (Siemens Molecular Imaging, Knoxville, TN). A transmission scan of 6 min using a single ^{137}Cs source was performed before the ^{18}F-AZD9272 injection. List-mode data were reconstructed with a series of 34 frames (20 s × 9, 1 min × 3, 3 min × 5, and 6 min × 17), using the ordinary Poisson-3D-ordered subset expectation maximization (OP-3D-OSEM) algorithm with 10 iterations and 16 subsets including modeling of the point spread function (PSF). Only a 105 min image of NHP1 was obtained due to the technical issue.

An automated blood sampling system (ABSS) was used to measure the continuous radioactivity for the first 3 min after the radioligand injection. Then, blood sampling was performed manually for the measurement of metabolism and radioactivity at 5, 15, 30, 60, 90, and 120 min after the injection. A reversed-phase radio-HPLC method was used to determine the amount of unchanged ^{18}F-AZD9272 and its radioactive metabolites in NHP plasma.[35]

https://dx.doi.org/10.1021/acschemneuro.9b00680
ACS Chem. Neurosci. 2020, 11, 1048−1057

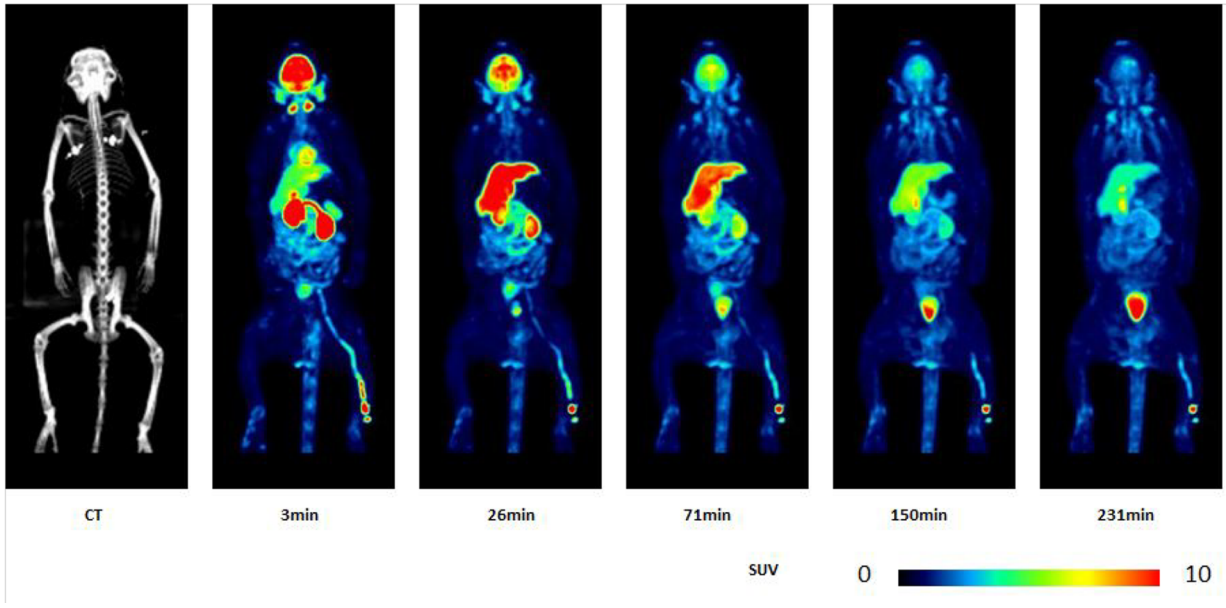

Figure 6. Whole body images of CT and PET.

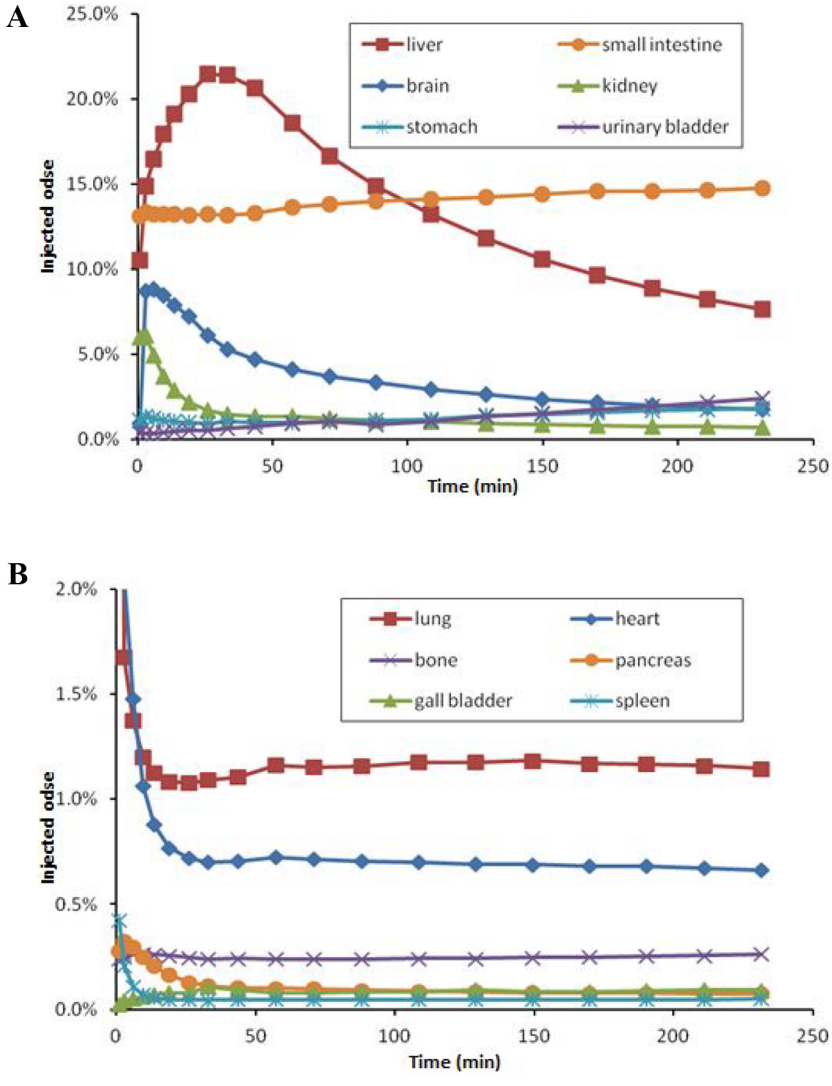

Figure 7. Time−activity curves of percent of injected dose: (A) high uptake organs and (B) low uptake organs.

https://dx.doi.org/10.1021/acschemneuro.9b00680
ACS Chem. Neurosci. 2020, 11, 1048−1057

Table 3. Estimated Radiation Dose at Different Organs

	NHP3 (μSv/MBq)	NHP4 (μSv/MBq)	mean (μSv/MBq)
adrenals	14.6	14.1	14.4
brain	13.0	17.4	15.2
breasts	8.0	7.9	7.9
gallbladder wall	21.3	21.1	21.2
LLI wall	26.8	27.9	27.4
small intestine	58.9	62.1	60.5
stomach wall	13.2	13.1	13.2
ULI wall	65.7	69.4	67.6
heart wall	17.5	19.0	18.3
kidneys	42.3	29.6	36.0
liver	47.0	45.7	46.4
lungs	12.7	11.8	12.3
muscle	10.1	10.0	10.1
ovaries	18.2	18.6	18.4
pancreas	16.4	15.4	15.9
red marrow	10.7	10.7	10.7
osteogenic cells	14.5	14.5	14.5
skin	7.4	7.4	7.4
spleen	9.6	8.4	9.0
testes	8.7	8.6	8.7
thymus	9.7	9.6	9.6
thyroid	9.1	9.1	9.1
urinary bladder wall	11.3	11.4	11.4
uterus	16.1	16.3	16.2
total body	12.2	12.1	12.2
effective dose	17.4	17.4	17.4

The regions of interest (ROIs) were delineated manually on the MRI images of each NHP for the anterior cingulate cortex, amygdala, caudate, cerebellum, hippocampus, insular cortex, occipital cortex, prefrontal cortex, putamen, temporal cortex, thalamus, ventral midbrain, and ventral striatum. The MRI of the individual NHP was co-registered to summed PET images of the whole measurement. By applying the co-registration parameters to ROIs, the time−activity curves of brain regions were generated from dynamic PET data.

As the main outcome measure, the total distribution volume (V_T) defined as $(K_1/k_2)(k_3/k_4 + 1)$ by the two tissue compartment (2TC) model and Logan graphical analysis (GA) was calculated with the metabolite corrected plasma radioactivity as the input function. The acquisition data was truncated to 63 min from 105 min (NHP1) or 123 min (NHP2) to check the time stability of V_T. The procedure has been described in detail in a previous publication on [^{11}C]AZD9272 binding.[33]

Whole Body PET. Two female cynomolgus monkeys (NHP3: 7420 g and NHP4: 6360 g) were used in this study. Anesthesia was induced by intramuscular injection of ketamine hydrochloride (approximately 10 mg/kg) at AFL and maintained by intravenous infusion of ketamine (4 mg/kg/h) and xylazine (0.4 mg/kg/h) with a pump. The body of the NHP was immobilized using a vacuum pad. Body temperature was maintained by using a Bair Hugger system (model 505, Arizant Healthcare, MN) and monitored with an esophageal thermometer. Heart rate, blood pressure, respiratory rate, and oxygen saturation were continuously monitored throughout the experiments. Fluid balance was maintained by continuous infusion of saline.

Whole-body PET scans were conducted using a GE Discovery PET/CT 710 system (GE Healthcare, Waukesha, WI). One low-dose CT scan was performed before intravenous administration of ^{18}F-AZD9272 for attenuation correction. Then five series of PET acquisitions, each covering five axial fields of view (AFOV), were conducted. The five PET series consisted of two 20 s × 5 AFOV, three 40 s × 5 AFOV, three 80 s × 5 AFOV, three 160 s × 5 AFOV, and eight 240 s × 5 AFOV. The total duration of the whole-body PET measurement was around 4 h. PET images were reconstructed with a 3D ordered-subset expectation maximization (OSEM) algorithm with three iterations and 18 subsets, including the time-of-flight information (VUE Point FX) and the point spread function correction (Sharp IR). A 2D Gaussian filter with 5.5 mm cutoff was used.

ROIs were drawn for the brain, heart, liver, lung, kidney, gall bladder, bone (lumbar vertebrae), urinary bladder, stomach, small intestine, spleen, and pancreas with the help of the CT images for anatomic landmarks. The time−activity curve was expressed as the percentage of the injected dose (%ID) calculated as follows: decay-corrected radioactivity (Bq/cc) × ROI volume (cc)/injected dose (Bq) × 100.

Estimates of the absorbed radiation dose in humans were calculated with OLINDA/EXM 1.1 (Organ Level INternal Dose Assessment Code) software, using the adult male (70 kg) reference model.[36] The fractional uptake in NHP organs was assumed to be equal to the uptake in human organs.

Radiometabolite Analysis. Radiometabolite analysis was performed following a previously published method.[35] In short, a reverse-phase HPLC method was used for the determination of the percentages of radioactivity corresponding to unchanged radioligand ^{18}F-AZD9272 and its radioactive metabolites during the course of a PET measurement. Venous blood samples (2 mL) were obtained from the monkey at different time point such as 5, 15, 30, 45, 60, 90, and 120 min after injection of ^{18}F-AZD9272. Collected blood (2 mL) was centrifuged at 2000*g* for 2 min to obtain the plasma (0.5 mL). The plasma obtained after centrifugation of blood at 2000*g* for 2 min was mixed with a 1.4 times volume of acetonitrile. The mixture was then centrifuged at 2000*g* for 4 min, and the extract was separated from the pellet and was diluted with water before injecting it into the HPLC system coupled to an online radioactivity detector. An Agilent binary pump (Agilent 1200 series) coupled to a manual injection valve (7725i, Rheodyne), 1−3.0 mL loop and a radiation detector (Oyokoken, S-2493Z) housed in a shield of 50 mm thick lead was used for metabolite measurements. Data collection and control of the LC system was performed using chromatographic software (ChemStation Rev. B.04.03; Agilent). The accumulation time of the radiation detector was 10 s. Chromatographic separation was achieved on an ACE C18 column (250 mm × 10 mm I.D) by gradient elution. Acetonitrile (A) and 10 mM ammonium format (B) were used as the mobile phase at 5.0 mL/min, according to the following program: 0−8.5 min, (A/B) 50:50 → 95:5 v/v; 8.5−11.0 min, (A/B) 95:5 v/v. Peaks for radioactive compounds eluting from the column were integrated, and their areas were expressed as a percentage of the sum of the areas of all detected radioactive compounds (decay-corrected to the time of injection on the HPLC).

To calculate the recovery of radioactivity from the system, an aliquot (2 mL) of the eluate from the HPLC column was measured and divided with the amount of total injected radioanalytes.

AUTHOR INFORMATION

Corresponding Author

Sangram Nag − *Department of Clinical Neuroscience, Center for Psychiatry Research, Karolinska Institutet and Stockholm County Council, Stockholm 17176, Sweden;* orcid.org/0000-0003-3590-4256; Phone: +46735431585; Email: sangram.nag@ki.se

Authors

Katarina Varnäs − *Department of Clinical Neuroscience, Center for Psychiatry Research, Karolinska Institutet and Stockholm County Council, Stockholm 17176, Sweden*

Ryosuke Arakawa − *Department of Clinical Neuroscience, Center for Psychiatry Research, Karolinska Institutet and Stockholm County Council, Stockholm 17176, Sweden*

https://dx.doi.org/10.1021/acschemneuro.9b00680
ACS Chem. Neurosci. 2020, 11, 1048−1057

Mahabuba Jahan − *Department of Medicinal Chemistry, Uppsala University, Uppsala 751 05, Sweden*

Magnus Schou − *Department of Clinical Neuroscience, Center for Psychiatry Research, Karolinska Institutet and Stockholm County Council, Stockholm 17176, Sweden; PET Science Centre, Precision Medicine, Oncology R&D, AstraZeneca, Stockholm 17176, Sweden;* orcid.org/0000-0002-4314-2418

Lars Farde − *Department of Clinical Neuroscience, Center for Psychiatry Research, Karolinska Institutet and Stockholm County Council, Stockholm 17176, Sweden*

Christer Halldin − *Department of Clinical Neuroscience, Center for Psychiatry Research, Karolinska Institutet and Stockholm County Council, Stockholm 17176, Sweden; Lee Kong Chian School of Medicine, Nanyang Technological University, Singapore 639798*

Complete contact information is available at: https://pubs.acs.org/10.1021/acschemneuro.9b00680

Author Contributions

The manuscript was written through contributions of all authors. All authors have given approval to the final version of the manuscript.

Notes

The authors declare no competing financial interest.

■ ACKNOWLEDGMENTS

The authors would like to thank AstraZeneca R&D for providing the precursor and reference standard. This work was supported by a grant from the Swedish Research Council [Grant Number 2015-02398]. We are grateful to all members of the PET group at the Karolinska Institutet.

■ ABBREVIATIONS

mGluR5, metabotropic glutamate receptor; PET, positron emission tomography; PD, Parkinson's disease; NHP, nonhuman primate; HPLC, high performance liquid chromatography; LC-MS, liquid chromatography−mass spectrometry; DMSO, dimethyl sulfoxide; DMF, dimethylformamide; PBS, phosphate buffered solution; MA, molar activity; HRRT, High Resolution Research Tomograph; SUV, standard uptake value; ROI, region of interest; V_T, distribution volume; TC, tissue compartment; GA, graphical analysis

■ REFERENCES

(1) Brassai, A., Suvanjeiev, R. G., Ban, E. G., and Lakatos, M. (2015) Role of synaptic and nonsynaptic glutamate receptors in ischaemia induced neurotoxicity. *Brain Res. Bull. 112*, 1−6.

(2) Petroff, O. A. C. (2002) GABA and glutamate in the human brain. *Neuroscientist 8* (6), 562−573.

(3) Abe, T., Sugihara, H., Nawa, H., Shigemoto, R., Mizuno, N., and Nakanishi, S. (1992) Molecular Characterization of a Novel Metabotropic Glutamate Receptor Mglur5 Coupled to Inositol Phosphate/Ca2+ Signal Transduction. *J. Biol. Chem. 267* (19), 13361−13368.

(4) Meldrum, B. S. (2000) Glutamate as a neurotransmitter in the brain: Review of physiology and pathology. *J. Nutr. 130* (4), 1007s−1015s.

(5) Cleva, R. M., and Olive, M. F. (2011) Positive Allosteric Modulators of Type 5 Metabotropic Glutamate Receptors (mGluR5) and Their Therapeutic Potential for the Treatment of CNS Disorders. *Molecules 16* (3), 2097−2106.

(6) Hoffpauir, B. K., and Gleason, E. L. (2002) Activation of mGluR5 modulates GABA(A) receptor function in retinal amacrine cells. *J. Neurophysiol. 88* (4), 1766−1776.

(7) Kerner, J. A., Standaert, D. G., Penney, J. B., Young, A. B., and Landwehrmeyer, G. B. (1997) Expression of group one metabotropic glutamate receptor subunit mRNAs in neurochemically identified neurons in the rat neostriatum, neocortex, and hippocampus. *Mol. Brain Res. 48* (2), 259−269.

(8) Shigemoto, R., Nomura, S., Ohishi, H., Sugihara, H., Nakanishi, S., and Mizuno, N. (1993) Immunohistochemical localization of a metabotropic glutamate-receptor, MgluR5, in the rat-brain. *Neurosci. Lett. 163* (1), 53−57.

(9) Romano, C., vandenPol, A. N., and O'Malley, K. L. (1996) Enhanced early developmental expression of the metabotropic glutamate receptor mGluR5 in rat brain: Protein, mRNA splice variants, and regional distribution. *J. Comp. Neurol. 367* (3), 403−412.

(10) Schoepp, D. D. (2001) Unveiling the functions of presynaptic metabotropic glutamate receptors in the central nervous system. *J. Pharmacol. Exp. Ther. 299* (1), 12−20.

(11) Rouse, S. T., Marino, M. J., Bradley, S. R., Awad, H., Wittmann, M., and Conn, P. J. (2000) Distribution and roles of metabotropic glutamate receptors in the basal ganglia motor circuit: implications for treatment of Parkinson's Disease and related disorders. *Pharmacol. Ther. 88* (3), 427−435.

(12) Breysse, N., Baunez, C., Spooren, W., Gasparini, F., and Amalric, M. (2002) Chronic but not acute treatment with a metabotropic glutamate 5 receptor antagonist reverses the akinetic deficits in a rat model of parkinsonism. *J. Neurosci. 22* (13), 5669−5678.

(13) Spooren, W. P. J. M., Vassout, A., Neijt, H. C., Kuhn, R., Gasparini, F., Roux, S., Porsolt, R. D., and Gentsch, C. (2000) Anxiolytic-like effects of the prototypical metabotropic glutamate receptor 5 antagonist 2-methyl-6-(phenylethynyl)pyridine in rodents. *J. Pharmacol. Exp. Ther. 295* (3), 1267−1275.

(14) Klodzinska, A., Tatarczynska, E., Chojnacka-Wojcik, E., Nowak, G., Cosford, N. D. P., and Pilc, A. (2004) *Neuropharmacology 47*, 342; (2004) *Neuropharmacology 47* (7), 1115−1115.

(15) Feyissa, A. M., Chandran, A., Stockmeier, C. A., and Karolewicz, B. (2009) Reduced levels of NR2A and NR2B subunits of NMDA receptor and PSD-95 in the prefrontal cortex in major depression. *Prog. Neuro-Psychopharmacol. Biol. Psychiatry 33* (1), 70−75.

(16) Ohnuma, T., Augood, S. J., Arai, H., McKenna, P. J., and Emson, P. C. (1998) Expression of the human excitatory amino acid transporter 2 and metabotropic glutamate receptors 3 and 5 in the prefrontal cortex from normal individuals and patients with schizophrenia. *Mol. Brain Res. 56* (1−2), 207−217.

(17) Yuksel, C., and Ongur, D. (2010) Magnetic Resonance Spectroscopy Studies of Glutamate-Related Abnormalities in Mood Disorders. *Biol. Psychiatry 68* (9), 785−794.

(18) Krystal, J. H., Mathew, S. J., D'Souza, D. C., Garakani, A., Gunduz-Bruce, H., and Charney, D. S. (2010) Potential Psychiatric Applications of Metabotropic Glutamate Receptor Agonists and Antagonists. *CNS Drugs 24* (8), 669−693.

(19) Chung, G., Kim, C. Y., Yun, Y. C., Yoon, S. H., Kim, M. H., Kim, Y. K., and Kim, S. J. (2017) Upregulation of prefrontal metabotropic glutamate receptor 5 mediates neuropathic pain and negative mood symptoms after spinal nerve injury in rats. *Sci. Rep. 7* (1), 9743−9755.

(20) Terbeck, S., Akkus, F., Chesterman, L. P., and Hasler, G. (2015) The role of metabotropic glutamate receptor 5 in the pathogenesis of mood disorders and addiction: combining preclinical evidence with human Positron Emission Tomography (PET) studies. *Front. Neurosci. 9*, 1−86.

(21) Tamagnan, G. D., Batis, J., Koren, A. O., Lee, H., Alagille, D., Jennings, D., Russell, D., Carson, R., Marek, K., and Seibyl, J. P. (2009) Initial human studies of [18F]-FPEB, a selective metabotropic glutamate receptor 5. *Eur. J. Nucl. Med. Mol. I 36*, S223−S223.

(22) Treyer, V., Streffer, J., Ametamey, S. M., Bettio, A., Blauenstein, P., Schmidt, M., Gasparini, F., Fischer, U., Hock, C., and Buck, A. (2008) Radiation dosimetry and biodistribution of 11C-ABP688 measured in healthy volunteers. *Eur. J. Nucl. Med. Mol. Imaging 35* (4), 766−770.
(23) Lucatelli, C., Honer, M., Salazar, J. F., Ross, T. L., Schubiger, P. A., and Ametamey, S. M. (2009) Synthesis, radiolabeling, in vitro and in vivo evaluation of [F-18]-FPECMO as a positron emission tomography radioligand for imaging the metabotropic glutamate receptor subtype 5. *Nucl. Med. Biol. 36* (6), 613−622.
(24) Yu, M. X., Tueckmantel, W., Wang, X. K., Zhu, A. J., Kozikowski, A. P., and Brownell, A. L. (2005) Methoxyphenylethynyl, methoxypyridylethynyl and phenylethynyl derivatives of pyridine: synthesis, radiolabeling and evaluation of new PET ligands for metabotropic glutamate subtype 5 receptors. *Nucl. Med. Biol. 32* (6), 631−640.
(25) Hamill, T. G., Krause, S., Ryan, C., Bonnefous, C., Govek, S., Seiders, T. J., Cosford, N. D. P., Roppe, J., Kamenecka, T., Patel, S., Gibson, R. E., Sanabria, S., Riffel, K., Eng, W. S., King, C., Yang, X. Q., Green, M. D., O'Malley, S. S., Hargreaves, R., and Burns, H. D. (2005) Synthesis, characterization, and first successful monkey imaging studies of metabotropic glutamate receptor subtype 5 (mGluR5) PET radiotracers. *Synapse 56* (4), 205−216.
(26) Brown, A. K., Simeon, F., Liow, J. S., Zoghbi, S., Kimara, Y., Fujita, M., MoZley, P. D., Pike, V., and Innis, R. B. (2008) Radiation dosimetry and human brain imaging of [F-18]SP203: A PET radioligand for the metabotropic glutamate mG1uR5 receptor. *NeuroImage 41*, T178−T178.
(27) Simeon, F. G., Brown, A. K., Zoghbi, S. S., Patterson, V. M., Innis, R. B., and Pike, V. W. (2007) Synthesis and simple F-18-labeling of 3-fluoro-5-(2-(2-(fluoromethyl)thiazol-4-yl)ethynyl)-benzonitrile as a high affinity radioligand for imaging monkey brain metabotropic glutamate subtype-5 receptors with positron emission tomography. *J. Med. Chem. 50* (14), 3256−3266.
(28) Simeon, F. G., Liow, J. S., Zhang, Y., Hong, J. S., Gladding, R. L., Zoghbi, S. S., Innis, R. B., and Pike, V. W. (2012) Synthesis and characterization in monkey of [C-11]SP203 as a radioligand for imaging brain metabotropic glutamate 5 receptors. *Eur. J. Nucl. Med. Mol. Imaging 39* (12), 1949−1958.
(29) Honer, M., Stoffel, A., Kessler, L. J., Schubiger, P. A., and Ametamey, S. M. (2007) Radiolabeling and in vitro and in vivo evaluation of [F-18]-FE-DABP688 as a PET radioligand for the metabotropic glutamate receptor subtype 5. *Nucl. Med. Biol. 34* (8), 973−980.
(30) Raboisson, P., Breitholtz-Emanuelsson, A., Dahllof, H., Edwards, L., Heaton, W. L., Isaac, M., Jarvie, K., Kers, A., Minidis, A. B. E., Nordmark, A., Sheehan, S. M., Slassi, A., Strom, P., Terelius, Y., Wensbo, D., Wilson, J. M., Xin, T., and McLeod, D. A. (2012) Discovery and characterization of AZD9272 and AZD6538-Two novel mGluR5 negative allosteric modulators selected for clinical development. *Bioorg. Med. Chem. Lett. 22* (22), 6974−6979.
(31) Andersson, J. D., Seneca, N., Truong, P., Wensbo, D., Raboisson, P., Farde, L., and Halldin, C. (2013) Palladium mediated C-11-cyanation and characterization in the non-human primate brain of the novel mGluR5 radioligand [C-11]AZD9272. *Nucl. Med. Biol. 40* (4), 547−553.
(32) Varnas, K., Cselenyi, Z., Arakawa, R., Nag, S., Stepanov, V., Moein, M. M., Johnstrom, P., Kingston, L., Elmore, C. S., Halldin, C., and Farde, L. (2020) The pro-psychotic metabotropic glutamate receptor compounds fenobam and AZD9272 share binding sites with monoamine oxidase-B inhibitors in humans. *Neuropharmacology 162*, 107809.
(33) Varnas, K., Jureus, A., Finnema, S. J., Johnstrom, P., Raboisson, P., Amini, N., Takano, A., Stepanov, V., Halldin, C., and Farde, L. (2018) The metabotropic glutamate receptor 5 radioligand C-11 AZD9272 identifies unique binding sites in primate brain. *Neuropharmacology 135*, 455−463.
(34) Zanotti-Fregonara, P., Lammertsma, A. A., and Innis, R. B. (2013) Suggested pathway to assess radiation safety of F-18-labeled PET tracers for first-in-human studies. *Eur. J. Nucl. Med. Mol. Imaging 40* (11), 1781−1783.
(35) Moein, M. M., Nakao, R., Amini, N., Abdel-Rehim, M., Schou, M., and Halldin, C. (2019) Sample preparation techniques for radiometabolite analysis of positron emission tomography radioligands; trends, progress, limitations and future prospects. *TrAC, Trends Anal. Chem. 110*, 1−7.
(36) Stabin, M. G. (2005) Blood-based red marrow dosimetry: Where's the beef? - Reply. *J. Nucl. Med. 46* (8), 1404−1406.

https://dx.doi.org/10.1021/acschemneuro.9b00680
ACS Chem. Neurosci. 2020, 11, 1048−1057